JOURNAL OF SPACECRAFT AND ROCKETS
Vol. 41, No. 4, July–August 2004

Robust Spacecraft Attitude Determination Using Global Positioning System Receivers

Jared Madsen* and E. Glenn Lightsey†
University of Texas at Austin, Austin, Texas 78712-1085

This work presents the development of a new attitude determination system based on global positioning system signals. This new algorithm utilizes signal-to-noise-ratio measurements from canted antennas to produce three-axis attitude solutions. These solutions are then used to determine the integer ambiguities for double-difference carrier-phase measurements. The two measurement types are processed through an extended Kalman filter to produce attitude solutions. The algorithm is tested using both hardware-in-the-loop orbit simulations and static rooftop data. These experiments demonstrate the speed of the integer resolution process and the accuracy of the resulting carrier-phase attitude solutions. Further tests demonstrate that the canting of the antennas has little or no effect on the double-difference carrier-phase measurements for antenna baselines of 1 m. The algorithm is modified to include magnetometer measurements. Simulation demonstrates how this addition further improves the integer resolution. The results of the rooftop and simulation experiments demonstrate that this new algorithm can quickly and accurately resolve the integer ambiguities associated with carrier-phase attitude determination. Once the integers are resolved, the resulting algorithm generates solutions of less than 0.5 deg in accuracy. To conclude this work, some possible future work is discussed.

Nomenclature

$\boldsymbol{A}_m$	=	magnetometer attitude matrix
a	=	mean radius of the Earth, 6371.2 km
a_i	=	calibration line fit coefficients
$\boldsymbol{B}$	=	traditional magnetic field vector, G
$\boldsymbol{b}_j$	=	antenna separation baseline vector in body coordinates, cycles
$\boldsymbol{b}_k$	=	antenna boresight vector in body coordinates, unit vector
$\boldsymbol{b}_m$	=	measured magnetic field vector, G
$\boldsymbol{H}$	=	matrix of partial derivatives
h	=	measurement model
h_n^m, g_n^m	=	Gauss coefficients
I_x, I_y, I_z	=	principal moments of inertia, kg · m^2
$\boldsymbol{K}$	=	Kalman gain vector
k	=	scaling factor on carrier-phase measurement noise term
k_{ij}	=	integer ambiguity for ith baseline and jth global positioning system (GPS) satellite
$\boldsymbol{l}$	=	GPS line-of-sight vector, unit vector
$\boldsymbol{P}$	=	7×7 covariance matrix
$P_n^m(\cos\theta)$	=	n Schmidt quasi-normalized associated Legendre functions of degree n and order m, $n \geq 1$ and $m \leq n$
$\boldsymbol{Q}$	=	7×7 process noise matrix
$\boldsymbol{q}$	=	4×1 quaternion
r	=	measurement noise
r_m	=	geocentric radius, km
S	=	number of SNR measurements in each double-difference measurement (4)
T_x, T_y, T_z	=	external torques, N · m
V	=	geomagnetic potential function
$\boldsymbol{x}$	=	seven-element state vector
$\bar{x}$	=	three-element subset of state vector, q_1, q_2, q_3
$\boldsymbol{x}_{\text{cal}}$	=	four-element calibration state vector
β_j	=	line bias, cycles
Δr	=	projected baseline range along line-of-sight vector, cycles
$\Delta\phi_{ij}$	=	single-difference carrier-phase measurement, cycles
θ, ϕ	=	geocentric spherical coordinates, rad
ν	=	noise term
$\boldsymbol{\omega}$	=	noise vector
ω_x, ω_y, ω_z	=	body rates, rad/s
$\nabla\Delta\phi_{ijk}$	=	double-difference carrier-phase measurement, cycles

Received 19 March 2003; revision received 30 June 2003; accepted for publication 30 June 2003.

*Ph.D., Department of Aerospace Engineering and Engineering Mechanics, WRW 412.

†Assistant Professor, Department of Aerospace Engineering and Engineering Mechanics, WRW 412. Senior Member AIAA.

Introduction

THE global positioning system (GPS) has demonstrated the ability to provide accurate navigation and attitude determination for spacecraft. Typically, attitude solutions are determined by estimating relative antenna positions in the external frame using single- or double-difference carrier-phase measurements.[1–7] Alternatively, attitude information can be obtained by measuring signal-to-noise ratios (SNR) and estimating antenna boresight vectors. This method has been explored by Axelrad and Behre[8] to generate single vector pointing solutions. It was also utilized by Dunn and Duncan[9] to obtain vector pointing solutions on the Microlab-1 satellite that were reported to be within 15 deg of truth. Work has also been done to obtain three-axis attitude estimates from the SNR measurements. Buist et al. obtained three-axis attitude solutions from a single GPS antenna, where the dynamics of the vehicle and the presence of a boom allowed for the resolution of all three axes of information.[10] Lightsey and Madsen have also obtained three-axis attitude solutions by using multiple canted antennas.[11,12]

Each of the GPS attitude determination methods has its own shortcomings. The SNR approach is generally only capable of providing coarse attitude solutions on the order of several degrees. Carrier-phase solutions are generally more accurate, but they are also less robust. Carrier-phase systems must resolve the unknown number of integer carrier phase cycles between antennas in order to generate solutions. Numerous methods have been developed to determine these integers. These methods, however, are generally complex, time consuming, and computationally expensive. These methods can also produce incorrect integers, which lead to erroneous attitude solutions.

This paper presents the development of a new algorithm, which was designed to overcome several of these shortcomings. This is accomplished by combining the two solution approaches into a single more robust attitude determination system via an extended Kalman filter. This combined algorithm takes advantage of the complementary nature of the two measurement types to produce a better overall algorithm. To improve the integer resolution process, the algorithm utilizes SNR measurements from multiple canted antennas to generate an attitude solution. The integer ambiguities are then estimated using this SNR attitude solution.

The resulting residuals from the estimated ambiguities are then tested to validate that they are correct. Once this validation has occurred, carrier-phase solutions are generated. Once carrier-phase solutions become available, the algorithm begins self-calibrating the antenna gain patterns. This improves the SNR solution accuracy in the event that the integers are lost.

This new algorithm is extensively tested using hardware-in-the-loop orbit simulation and static rooftop data. These experiments demonstrate that the SNR solutions are accurate enough to quickly resolve the integer ambiguities. The tests further reveal that the carrier-phase solutions are not adversely impacted by the canting of the antennas.

The algorithm is then modified to include measurements from a three-axis magnetometer. The addition of this measurement provides improved integer resolution in the orbit simulations.

The simulation and rooftop experiments validate that the new algorithm quickly and accurately resolves the integers associated with the carrier-phase measurements. In most tests the integers were resolved in under 30 s. Once the integers are resolved, the algorithm provides attitude estimates in the 0.5-deg accuracy range. In conclusion, some possible future work and hardware improvements are discussed.

Filtering

To combine the two measurement types, an extended Kalman filter (EKF) is utilized. The EKF is developed in detail by Gelb et al.[13] The basic equations are reproduced here for reference.

Model:

$$\dot{\boldsymbol{x}}(t) = f[\boldsymbol{x}(t), t] + \omega(t), \qquad E[\omega(t)\omega^T(\tau)] = \boldsymbol{Q}(t)\delta(t-\tau)$$

$$y = h[\boldsymbol{x}(t)] + \nu(t), \qquad E[\nu(t)\nu^T(\tau)] = r(t)\delta(t-\tau) \tag{1}$$

The measurement noise r and process noise $\boldsymbol{Q}$ terms are used to adjust the filter to improve performance.

Propagation:

$$\dot{\hat{\boldsymbol{x}}}(t) = f[\hat{\boldsymbol{x}}(t), t], \qquad \boldsymbol{A}[\hat{\boldsymbol{x}}(t)] = \left(\frac{\partial f}{\partial \boldsymbol{x}}\right)\bigg|_{x=\hat{x}}$$

$$\dot{\boldsymbol{P}}(t) = \boldsymbol{A}[\hat{\boldsymbol{x}}(t)]\boldsymbol{P}(t) + \boldsymbol{P}(t)\boldsymbol{A}^T[\hat{\boldsymbol{x}}(t)] + \boldsymbol{Q} \tag{2}$$

Update:

$$\hat{\boldsymbol{x}}(+) = \hat{\boldsymbol{x}}(-) + \boldsymbol{K}\{y - h[\hat{\boldsymbol{x}}(-)]\}$$

$$\boldsymbol{P}(+) = \{I - \boldsymbol{K}\boldsymbol{H}[\hat{\boldsymbol{x}}(-)]\}\boldsymbol{P}(-)$$

$$\boldsymbol{H}[\hat{\boldsymbol{x}}(-)] = \left(\frac{\partial h}{\partial \boldsymbol{x}}\right)\bigg|_{x=\hat{x}(-)}$$

$$\boldsymbol{K} = \boldsymbol{P}(-)\boldsymbol{H}^T[\hat{\boldsymbol{x}}(-)]\{\boldsymbol{H}[\hat{\boldsymbol{x}}(-)]\boldsymbol{P}(-)\boldsymbol{H}^T[\hat{x}(-)] + r\}^{-1} \tag{3}$$

The level of accuracy of the filter is directly related to the accuracy of the dynamic model employed. For all tests performed for this research, Euler's equations with principal moments of inertia were used to propagate the body rates forward in time:

$$\dot{\omega}_x = 1/I_x[(I_y - I_z)\omega_y\omega_z + T_x]$$

$$\dot{\omega}_y = 1/I_y[(I_z - I_x)\omega_x\omega_z + T_y]$$

$$\dot{\omega}_z = 1/I_z[(I_x - I_y)\omega_x\omega_y + T_z] \tag{4}$$

For this work there were no external torques (T_i). Specific applications might have external torques caused by gravity gradients, solar pressure, drag, and internal moving parts, among other sources. The accuracy with which these external torques are modeled will have a direct impact on the solution accuracy.

There are several methods available for attitude representation. The quaternion is generally the preferred method of representing spacecraft attitude and was chosen for use in this algorithm. For this paper the quaternion was defined in the following manner, where the quaternion represents a rotation through the angle θ about the unit vector $\boldsymbol{u}$[14]:

$$q_0 = \cos(\theta/2) \tag{5}$$

$$[q_1 \quad q_2 \quad q_3]^T = \boldsymbol{u}\sin(\theta/2) \tag{6}$$

The norm of the quaternion is one. To account for this requirement in the attitude estimation algorithm, the quaternion is normalized after each measurement update.

In addition to the quaternion, the body rates of the spacecraft are part of the attitude state. Therefore the state vector can be written as

$$\boldsymbol{x} = [q_0 \quad q_1 \quad q_2 \quad q_3 \quad \omega_x \quad \omega_y \quad \omega_z]^T \tag{7}$$

The quaternion is propagated according to the standard equation[14]:

$$\dot{\boldsymbol{q}} = \frac{1}{2}\begin{bmatrix} 0 & -\omega_x & -\omega_y & -\omega_z \\ \omega_x & 0 & \omega_z & -\omega_y \\ \omega_y & -\omega_z & 0 & \omega_x \\ \omega_z & \omega_y & -\omega_x & 0 \end{bmatrix}\boldsymbol{q} \tag{8}$$

SNR Measurement Updates

To utilize SNR measurements in the combined algorithm, they must be related to the quaternion state. The antenna boresight vectors are known in the body frame. A simple hemispherical model for the relationship between the boresight vector and the SNR measurement can be expressed as

$$\boldsymbol{l} \cdot \boldsymbol{b}_k = \cos(\alpha) = l_x b_x + l_y b_y + l_z b_z \tag{9}$$

where $\boldsymbol{l}$ is the known line-of-sight vector to the GPS satellite, $\boldsymbol{b}_k$ is the kth antenna boresight vector, and α is the angle between the two, as shown in Fig. 1. Solution accuracy can be improved by replacing $\cos(\alpha)$ with a calibration function generated by data from the antenna/receiver combination to be utilized in the system.[15]

A rotation of the vehicle generates a corresponding rotation on every antenna boresight. Therefore, the kth antenna boresight can be related to the vehicle state through the quaternion rotation operator[14]:

$$\boldsymbol{b}_k^{\text{rot}} = \left(2x_1^2 - 1\right)\boldsymbol{b}_k + 2(\bar{x}\cdot\boldsymbol{b}_k)\bar{x} + 2x_1(\bar{x}\times\boldsymbol{b}_k) \tag{10}$$

$$\bar{x} = [q_1 \quad q_2 \quad q_3] \tag{11}$$

The measurement model is the inner product between the rotated antenna boresight vector and the line-of-sight vector:

$$h = \boldsymbol{b}_k^{\text{rot}} \cdot \boldsymbol{l}_i \tag{12}$$

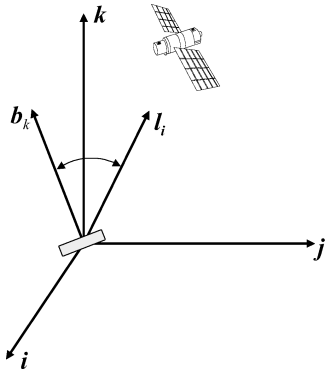

Fig. 1 SNR attitude determination vectors.

This equation is expanded and linearized to compute the $\boldsymbol{H}$ matrix [Eq. 13)]:

$$\boldsymbol{H}^T = 2 \cdot \begin{bmatrix} 2x_1b_1 + x_3b_3 - x_4b_2 & 2x_1b_2 + x_4b_1 - x_2b_3 & 2x_1b_3 + x_2b_2 - x_3b_1 \\ 2x_2b_1 + x_3b_2 + x_4b_3 & x_3b_1 - x_1b_3 & x_4b_1 + x_1b_2 \\ x_2b_2 + x_1b_3 & 2x_3b_2 + x_2b_1 + x_4b_3 & x_4b_2 - x_1b_1 \\ x_2b_3 - x_1b_2 & x_3b_3 + x_1b_1 & 2x_4b_3 + x_2b_1 + x_3b_2 \\ 0 & 0 & 0 \\ 0 & 0 & 0 \\ 0 & 0 & 0 \end{bmatrix} \cdot \boldsymbol{l} \tag{13}$$

Carrier-Phase Measurement Updates

In addition to the SNR measurements, the carrier-phase measurements must also be related to the vehicle state. The measured carrier phase can be related to the vector between the receiving antennas by the following equation (Fig. 2):

$$\Delta r = \boldsymbol{l} \cdot \boldsymbol{b}_j \tag{14}$$

Unfortunately, the total range between the antennas cannot be measured, only the fractional carrier-phase at each antenna, leaving an unknown number of integer carrier-phase cycles between the antennas. This number of cycle wavelengths is known as the integer ambiguity k. In addition to the integer ambiguity, the carrier phase measured at each antenna contains a bias term β. The bias is called the line bias and is primarily caused by the electrical line length from the antenna phase center to the point interior to the receiver where the measurement is actually made. There is also a measurement noise term ν.

With these new terms defined, the actual relationship between the measured carrier phase and the projected range can be written as

$$\Delta\phi_{ij} = \boldsymbol{l}_i \cdot \boldsymbol{b}_j - k_{ij} + \beta_j + \nu_i \tag{15}$$

where $\Delta\phi_{ij}$ is the actual differential carrier phase measurement, the subscript i refers to the GPS satellite, and the subscript j is the antenna baseline.

The line bias term can be removed by forming the double-difference phase measurement:

$$\nabla\Delta\phi_{ijk} = \Delta\phi_{ij} - \Delta\phi_{kj} = (\boldsymbol{l}_i - \boldsymbol{l}_k) \cdot [\boldsymbol{b}_j]_{\text{ext}} - (k_{ij} - k_{kj}) + (\nu_{ij} - \nu_{kj}) \tag{16}$$

This equation is quite similar to the measurement equation for the SNR solutions. Again, it can be related to the state through quaternion multiplication to form $\boldsymbol{b}_j^{\text{rot}}$ [eq. (10)]. This equation is then used to form the measurement model equation:

$$h = (\boldsymbol{l}_i - \boldsymbol{l}_k) \cdot \boldsymbol{b}_j^{\text{rot}} - (k_{ij} - k_{kj}) \tag{17}$$

This equation is expanded and linearized with respect to the state, similar to the SNR equation [Eq. (13)]. In fact, the result [Eq. (18)] is the same, except that $\boldsymbol{l}$ is replaced with $(\boldsymbol{l}_i - \boldsymbol{l}_k)$. The integer ambiguities do not appear in $\boldsymbol{H}$ because they are not part of the state vector:

$$\boldsymbol{H}^T = 2 \cdot \begin{bmatrix} 2x_1b_1 + x_3b_3 - x_4b_2 & 2x_1b_2 + x_4b_1 - x_2b_3 & 2x_1b_3 + x_2b_2 - x_3b_1 \\ 2x_2b_1 + x_3b_2 + x_4b_3 & x_3b_1 - x_1b_3 & x_4b_1 + x_1b_2 \\ x_2b_2 + x_1b_3 & 2x_3b_2 + x_2b_1 + x_4b_3 & x_4b_2 - x_1b_1 \\ x_2b_3 - x_1b_2 & x_3b_3 + x_1b_1 & 2x_4b_3 + x_2b_1 + x_3b_2 \\ 0 & 0 & 0 \\ 0 & 0 & 0 \\ 0 & 0 & 0 \end{bmatrix} \cdot (\boldsymbol{l}_i - \boldsymbol{l}_k) \tag{18}$$

Integer Resolution

To use the carrier-phase measurements, the unknown integer ambiguities k_{ij} must be determined. Once the integers are resolved, they are added directly to the h equation. As explained earlier, numerous search techniques are available for determining the integers by examining integer possibilities and comparing the resulting measurement residuals.

As an alternative, if the attitude of the vehicle is known a priori to a sufficiently high accuracy then the integers can simply be assigned. The required level of accuracy to correctly assign the integers is a function of the antenna baseline length, line-of-sight geometry, and noise on the carrier-phase measurements. For example, Fig. 3 shows the required in-plane accuracy to estimate correctly the integers as a function of baseline length for a carrier-phase measurement with 0.1 cycles of noise and a line-of-sight geometry perpendicular to the antenna baseline. The curve was determined by calculating the angle error between the true baseline and the estimated baseline that resulted in a change in the carrier-phase measurement of greater than 0.4 cycles. When a 0.1 noise value is added to this change, the resulting measurement would cause a rounded estimate of the integer to be incorrect.

The combined algorithm uses the SNR measurements from canted antennas to generate the a priori attitude estimate. After the SNR measurements have all been applied, the algorithm creates a temporary attitude state that is set equal to the SNR determined state. The integer ambiguities are then estimated by rounding the difference between the predicted measurement and the actual carrier-phase measurement to the nearest integer. This integer is then added to the carrier-phase measurement, and the measurement is used to update the temporary state. After all available carrier-phase measurements at one epoch are used to update the state, the measurement residuals are calculated. If the measurement residuals fall below a determined threshold, then the integers are assumed to have been correctly

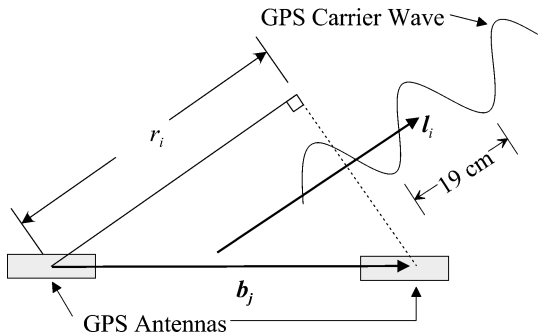

Fig. 2 Carrier-phase interferometry.

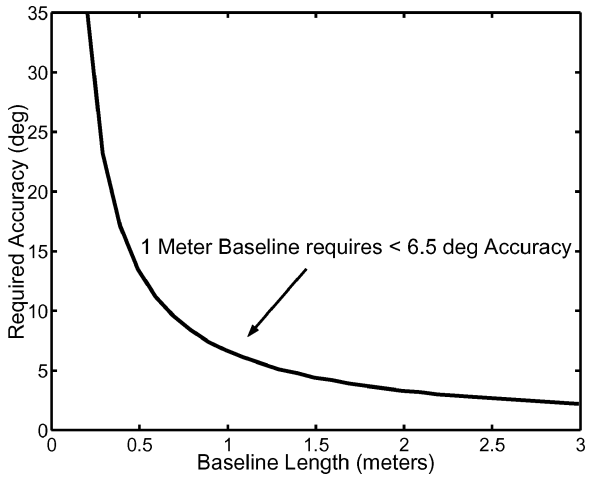

Fig. 3 Required angle accuracy for correct integer resolution.

assigned. The actual estimated state is set equal to the temporary state, and the carrier-phase measurements are utilized, as depicted in Fig. 4.

Once the integers have been assigned, the algorithm continues to check the residuals in order to detect any incorrect assignments. The carrier-phase measurements will continue to be used until the algorithm detects an incorrect assignment.

Antenna Gain Pattern Self-Calibration

For most applications the algorithm can provide SNR solutions with sufficient accuracy to resolve the integers by using the assumed cosine function gain pattern. As mentioned, however, a calibration function can be used to improve the integer resolution accuracy. Previous work has demonstrated that an on-orbit calibration can improve solution accuracy as long as the true attitude is within 10 deg of the estimated attitude during the calibration process.[11]

For antenna separations of approximately 1 m, the carrier-phase measurements provide attitude solutions that are generally accurate to the subdegree level. Therefore, the algorithm performs an antenna gain pattern self-calibration once the carrier-phase integers are resolved. This is accomplished by using a simple EKF filter to represent the coefficients of a polynomial fit. Namely, the calibration uses the following state vector and measurement equation:

$$\boldsymbol{x}_{\text{cal}} = [a_0 \quad a_1 \quad a_2 \quad a_3] \tag{19}$$

$$h = \boldsymbol{l}_i \cdot \boldsymbol{b}_k = a_0 + a_1(\text{SNR}) + a_2(\text{SNR})^2 + a_3(\text{SNR})^3 \tag{20}$$

From these two definitions $\boldsymbol{H}$ can be formed:

$$\boldsymbol{H} = [1 \quad \text{SNR} \quad \text{SNR}^2 \quad \text{SNR}^3] \tag{21}$$

This approach to the antenna calibration assumes that all satellites can be treated as the same. It also assumes symmetry around the antenna boresight. Both of these assumptions are true for most applications. If, however, an instance is anticipated where these assumptions might not be valid, then the algorithm could be modified to account for it. For example, if the antenna gain pattern is not axisymmetric, then the algorithm could be modified to perform a spherical harmonic calibration. Such a modification would increase the complexity of the algorithm. Additionally, the calibration value can be allowed to change over time. If a process noise $\boldsymbol{Q}$ value of zero is utilized, then at some point the calibration will stop changing. If, however, a larger value of process noise is used, then the calibration can always vary. For the experiments presented in this paper, a process noise value of zero was chosen.

By using a filter, an estimate of the calibration accuracy can be determined from the calibration covariance. Once the calibration covariance falls below a predetermined value, the calibration curve is used in performing attitude updates based on SNR measurements. This threshold is dependent on the receivers utilized, the SNR measurement units, and the determined accuracy required to improve the calibrated estimation of attitude based on SNR measurements.

Experimental Setup

To test the algorithm and adjust the necessary parameters to achieve good performance, two types of tests were run.

Simulation

Orbit simulation tests were conducted using a STR 4760 Multi-Channel GPS Signal simulator manufactured by Global Systems Simulations, Ltd. (GSSL, now Spirent Communications). The simulator uses GPS satellite orbits and a simulated receiver orbit to calculate idealized GPS signals. These signals include ionosphere effects, measurement noise, and signal strength variations based on a simulated hemispherical antenna receiving pattern. These computed radio frequency signals are then synthesized by the STR 4760 signal generator and fed directly into the GPS receiver through a coaxial cable, as illustrated in Fig. 5.

The measurements were made by a Space-Integrated GPS/INS Receiver (SIGI) at a 1-Hz sample rate. The SIGI receiver uses a Force-19 GPS receiver that has been modified by NASA engineers for space use. The SIGI receiver is manufactured by Honeywell, Inc. The SIGI uses six channels multiplexed across four antennas to take differential carrier-phase measurements and produce navigation and attitude solutions. For the purposes of this research, the SIGI receiver's ability to compute attitude solutions was not utilized; it was only used to obtain the raw measurements necessary for the algorithm to produce attitude solutions. The receiver measured SNR levels, line-of-sight vectors, and differential carrier phase. These measurements were saved to a file and then postprocessed through the algorithm. For these experiments a low Earth orbit ($a = 6678137$ m, $e = 0.001$, $i = 0$ deg) was simulated.

The simulations did not include any multipath effects. These effects were, however, present during the rooftop tests.

Rooftop

The second set of experiments was conducted using data collected on a roof. Three Micro Pulse 13700 Series Lightweight Survey antennas were attached to a pipe-mounted antenna array. The array is 1 m on a side. Each antenna connects to a bolt that is attached to a polyvinyl chloride (PVC) pipe T-joint. The T-joints can be rotated and set in place with set screws. The pipe upon which each T-joint rotates was measured and marked with various angles. This experimental setup is shown in the photo in Fig. 6. The antennas were then connected to a SIGI receiver that again recorded the measured SNR levels, line-of-sight vectors, and differential phase measurements.

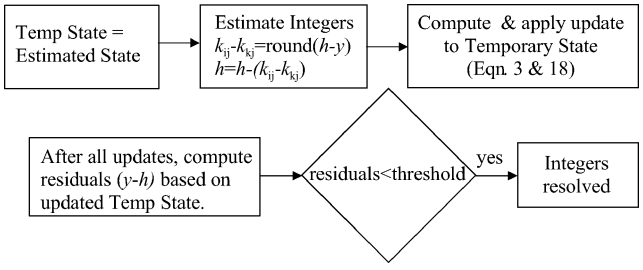

Fig. 4 Integer resolution logic.

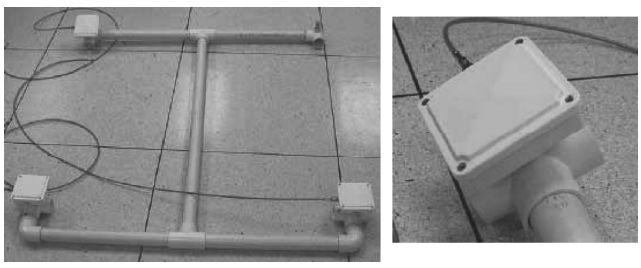

Fig. 6 PVC antenna array with closeup.

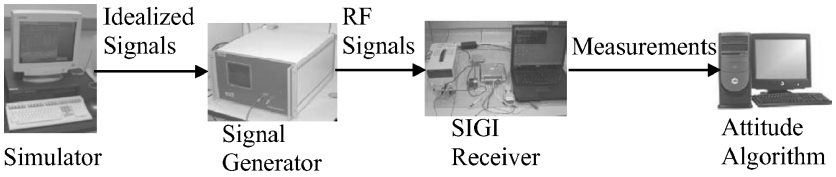

Fig. 5 Simulation setup.

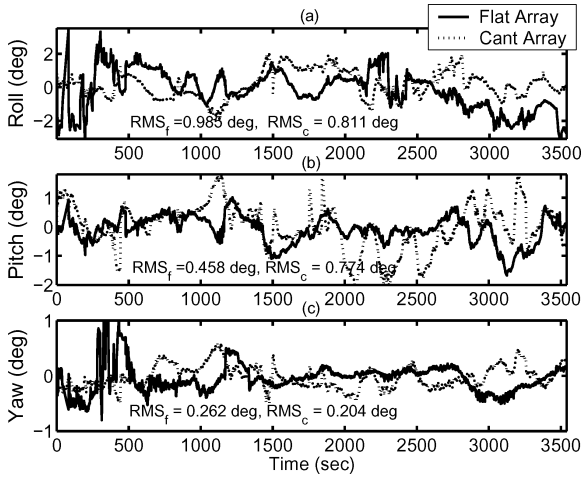

Fig. 7 Attitude estimates, flat vs 15-deg canted antenna array: a) roll, b) pitch, and c) yaw.

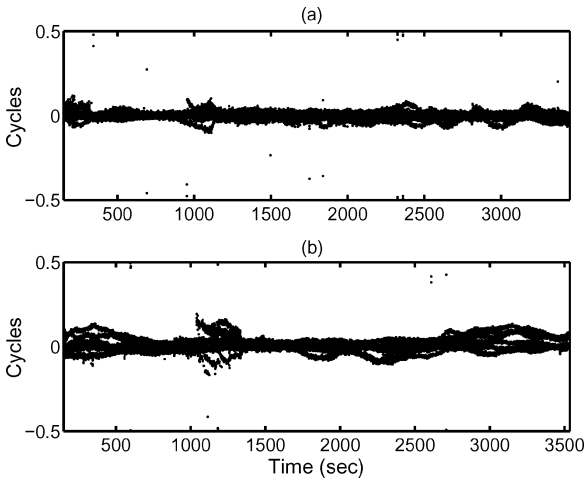

Fig. 8 Carrier-phase measurement residuals: a) 15-deg canted array, and b) flat array.

These measurements were saved to a file and then postprocessed with the algorithm.

The array experiments were limited to three antennas because of some hardware issues at the time of the tests. It became apparent that one rf input to the SIGI receiver that was available was malfunctioning and did not generate reliable measurements. The attitude algorithm will generate more accurate results if more antennas are utilized, but it is capable of producing carrier-phase attitude solutions with as few as two antennas.

Results

It has been previously proposed that canted antennas can produce changes in carrier-phase measurements.[1] To investigate this possibility, a test was conducted. The rooftop array was setup with aligned antennas and allowed to take measurements for several hours. The antennas were then canted at 15 deg and allowed to take measurements on a different day. The resulting attitude solutions and measurement residuals were then compared. The results, shown in Figs. 7 and 8, do not reveal any trends or changes that would be indicative of a change in the carrier-phase measurements as a result of canting the antennas. The results are not identical primarily because of differences in the GPS satellite geometries during the two tests. The measurements themselves were used to perform a self-survey on each set of baselines. This removes any biases that might have been introduced by the canting of the antennas. It seems apparent from the results that as long as a self-survey is utilized to determine the antenna baselines then canted antennas on a 1-m baseline array do not have a significant effect on the double-difference carrier-phase measurements. This conclusion is further verified by the resulting attitude accuracy of longer duration tests, which are presented later in this research.

Table 1 Integer resolution thresholds (minimum of eight simultaneous measurements)

Max σ, cycles	Missed opportunity, %	Incorrect assignment, %
0.06	8.78	2.41
0.05	10.09	1.35
0.45	11.29	1.01
0.04	12.65	0.48
0.035	15.48	0.00

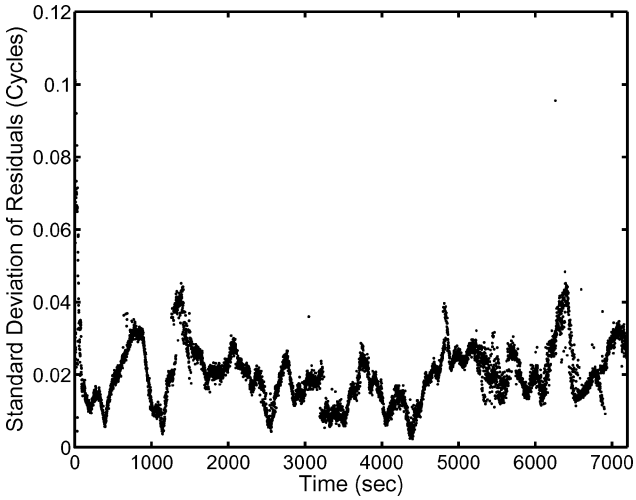

Fig. 9 Standard deviation of residuals during correct integer lock.

Tests were conducted to determine the measurement residual level at which the integers could be correctly assigned. This threshold was set by using the array on the roof with antennas canted at 15 deg. Data were collected for 2 h. The standard deviation of the computed residuals was used as the threshold for integer resolution. The threshold was varied, and the percentages of incorrect assignment and missed opportunities were calculated. The results appear in Table 1.

As expected, a lower threshold increases the number of times that the integers are actually correct but not assigned. It also decreases the possibility of an incorrect assignment. To attempt to guarantee correct integer assignment, a threshold of eight simultaneous measurements with a standard deviation of less than 0.035 cycles was chosen for the remaining tests. The threshold chosen is dependent on the accuracy of the carrier-phase measurement and the noise environment in which the receiver is deployed. The appropriate threshold to utilize for an individual application would need to be determined through testing of the specific hardware and environment.

Although the algorithm will not likely assign incorrect integers when properly adjusted, it is still desirable to continuously check the residuals in order to attempt to detect an incorrect assignment. To set the necessary threshold for this detection, the residuals were calculated during correct assignment and plotted in Fig. 9. This plot shows that during correct assignment the standard deviation of residuals is generally less than 0.04 cycles. On occasion, however, the standard deviation can be as high as 0.1 cycles because of anomalous readings. The incorrect assignment detection logic was determined based on this plot. If the standard deviation of residuals ever grows beyond the incorrect assignment threshold, then the algorithm sets a flag. If the residual falls below the lock threshold, then the flag is reset. If, however, the residuals are greater than the incorrect assignment threshold when the flag has been set, then the algorithm assumes the integers are lost. This logic is displayed in the flowchart in Fig. 10. This logic helps to improve the incorrect detection time while limiting the number of false detections. The incorrect assignment threshold was determined by setting the integers

Table 2 Incorrect integer assignment detection thresholds (rooftop test)

Max σ, cycles	Average detection time, s	Max detection time, s	% false detection
0.04	2.01	3	0.049
0.05	2.03	3	0.008
0.07	3.68	76	0.00
0.09	7.43	96	0.00
0.11	13.50	301	0.00

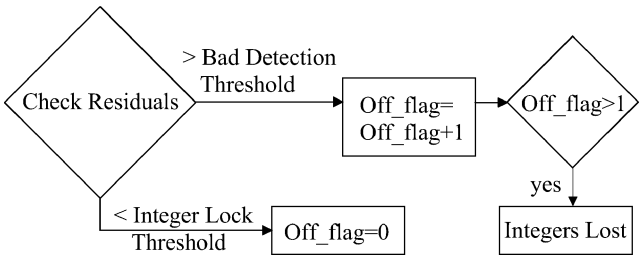

Fig. 10 Incorrect integer assignment detection logic.

incorrectly and then recording the average and maximum times to detection. The results appear in Table 2.

To eliminate false detections, the threshold was set at 0.07 cycles. Again, this number is environment dependent and might need to be adjusted for higher noise situations.

With the detection thresholds set, the filter parameters can be adjusted to achieve good performance. The purpose of the SNR solutions is to estimate the integer ambiguities quickly and accurately. Therefore, the SNR measurement parameters were based on the percentage of time that the SNR solutions were actually accurate enough to generate correct integer estimation. This test was again performed using rooftop data. The residual check outlined earlier prevents the algorithm from assigning incorrectly estimated integers. Based on this test, the filter parameters for the SNR measurements were set at $r = 0.1$ and $\boldsymbol{Q} = \boldsymbol{I} \cdot 3 \times 10^{-2}$.

The SIGI receiver used for the testing of this algorithm has several limitations in terms of SNR solution accuracy. Most significantly, the SIGI receiver quantizes its SNR measurements into coarse integer bins. Further, it records SNR in units known as AMU instead of the standard dB-Hz. AMU is defined by the receiver designer as an amplitude measurement unit. The means for converting between AMU and decibels-hertz is not well understood. Also, the SIGI receiver has only six channels to track GPS satellites. Many modern receivers have more.

The SIGI receiver was utilized for the testing of this algorithm because it was available and provided the necessary carrier-phase measurements between multiple antennas. It is possible, however, to improve the algorithm's performance if a receiver that makes a more accurate measurement of SNR is used.

NASA is developing a four-antenna receiver that is planned to have carrier-phase measurement capability. This receiver, known as the PiVoT,[16] currently only has code and SNR measurement capabilities. Tests conducted with the PiVoT receiver produced SNR attitude solutions with standard deviations of 1.57, 2.02, and 2.18 deg in roll, pitch, and yaw, respectively. If these solutions are substituted as the SNR solutions for the SIGI, then the integers are estimated correctly 97.7% of the time during the rooftop test when the calibration is used. A summary of the SNR integer resolution performance, comparing the PiVoT and SIGI receivers, appears in Table 3.

To set the parameters for the carrier-phase measurements, the same rooftop test was used. The rms error was chosen as the performance index for the tuning process. Previous work[17] has demonstrated that the carrier-phase measurement accuracy is a function of $1/\sqrt{\text{SNR}}$. Utilizing this result, it was determined that if the measurement noise value r was set according to the following equation,

Table 3 Integer resolution comparison: SIGI vs PiVoT

Receiver	Calibration	Correct integer estimation, %	Initial correct estimate, s
SIGI	No	51.0	40
SIGI	Yes	53.6	4
PiVoT	Yes	97.7	4

Table 4 Attitude error results summary

	Initial integer resolution, s		RMS attitude error, deg		
Test	Cal[a]	No cal	Roll	Pitch	Yaw
2 h, 15 deg: rooftop	14	40	0.440	0.429	0.149
6 h, 15 deg: rooftop	17	23	0.706	0.543	0.167
14 h, 15 deg: rooftop	42	36	0.465	0.451	0.150
4 h, 30 deg: rooftop	9	9	1.001	0.856	0.304
4.5 h, 30 deg: simulation	18	6	0.111	0.128	0.045

[a]cal = calibration.

then the results improved:

$$r = k^* \sum_{n=1}^{S} \frac{1}{\sqrt{\text{SNR}_n}} \tag{22}$$

The best performance, as judged by rms values, occurred when $\boldsymbol{Q}_{\text{diag}}$ was set to zero. At this setting, however, the filter converged to nonzero values for the body rates. This would cause the filter solutions to diverge over time. Therefore, for the remaining tests values of $k = 0.6$ and $\boldsymbol{Q}_{\text{diag}} = 8 \cdot 10^{-14}$ were used. It was also found that waiting for 2 min after the integers were resolved to change from the SNR $\boldsymbol{Q}$ value to the carrier-phase value improved performance by allowing the rates to approach correct values before the covariance began shrinking significantly. It was also found that discontinuing SNR measurement updates once the carrier-phase integers were resolved improved overall solution accuracy marginally.

With the filters correctly tuned, multiple tests on the roof and on the simulator were performed to validate the algorithm's performance. The results appear in Table 4. The yaw results are consistently better than the other results because the GPS satellites are always above the array, and hence the yaw rotation is always more well defined than the pitch and roll. The major error source in all of the results is multipath, which is environment and GPS satellite geometry dependent. The characteristic oscillations in some of the results are typical of multipath error sources. The increased error for the 6-h test is a result of a noisy section of results that was likely caused by a bad multipath geometry. The canting of the antennas has a tendency to increase the error associated with the multipath environment. This is because the antennas are canted from zenith toward the horizon and thus are more likely to record signals reflected off the roof. This is illustrated in the increased error seen in the 30-deg canting experiment. Doubling the canting angle resulted in nearly doubling the rms errors. For specific applications measures can be taken to mitigate the multipath environment seen by canted antennas.

Plots of the 14-h test appear in Figs. 11–13. These plots are representative of all of the outside tests. The simulation results are, as expected, less noisy.

Magnetometer Combination

The algorithm structure allows for additional sensor integration. To demonstrate this possibility, the algorithm was modified to include magnetometer data.

Magnetometer Measurement Updates

A three-axis magnetometer measures the Earth's magnetic field direction and magnitude in the spacecraft body coordinates. This measurement is then compared to a model of the Earth's magnetic

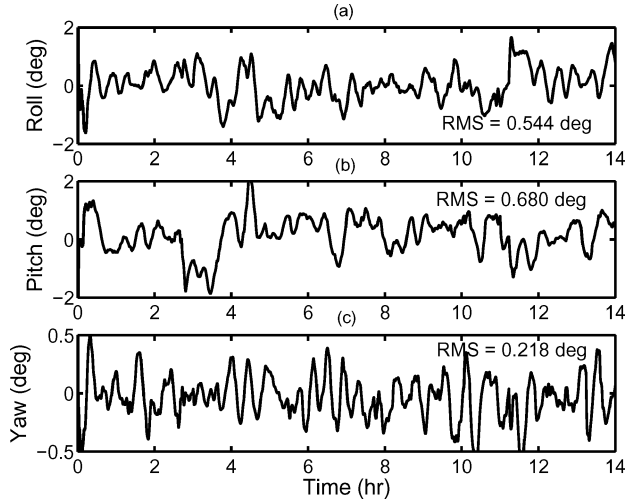

Fig. 11 Rooftop attitude estimation: a) roll, b) pitch, and c) yaw.

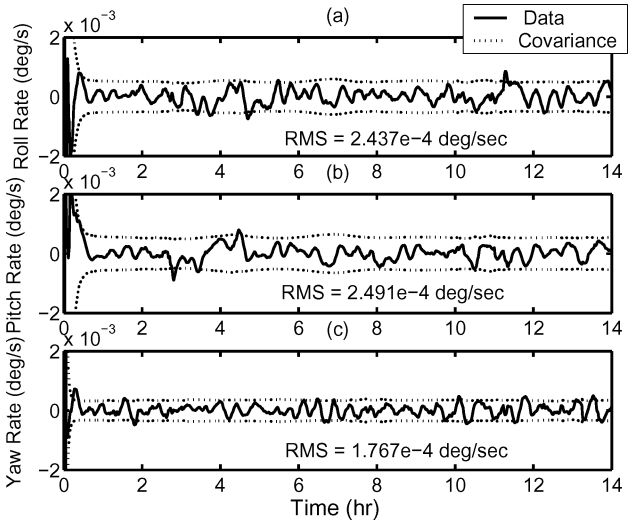

Fig. 12 Rooftop body rate estimation error with covariance: a) roll rate, b) pitch rate, and c) yaw rate.

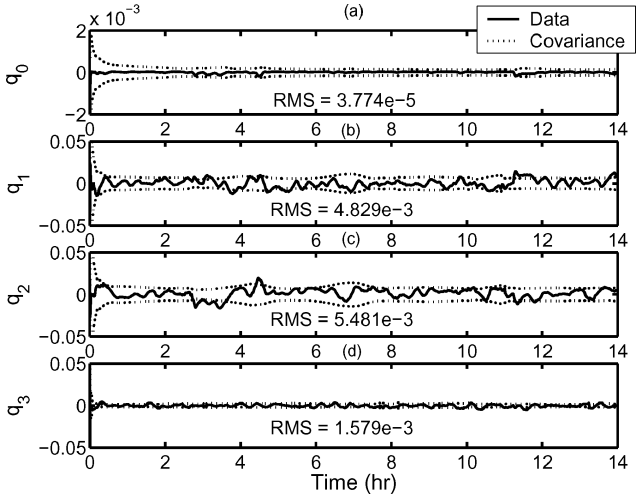

Fig. 13 Rooftop quaternion estimation error with covariance: a) q_0, b) q_1, c) q_2, and d) q_3.

field. The difference between these two is used to determine the attitude of the vehicle. The representative equation is

$$\boldsymbol{B}_b = \boldsymbol{A}_m \boldsymbol{B}_I + \nu \tag{23}$$

To incorporate the magnetometer measurements, it is again necessary to relate the measurement to the vehicle state. This is simply the expected magnetic field vector, based on the Earth magnetic model, for a nominally pointed spacecraft transformed through the present estimated vehicle attitude. This is again done using quaternion multiplication, in this instance to express the measured value in terms of the external reference frame:

$$\boldsymbol{b}_m^{\text{rot}} = \left(2x_1^2 - 1\right)\boldsymbol{b}_m + 2(\bar{x} \cdot \boldsymbol{b}_m)\bar{x} - 2x_1(\bar{x} \times \boldsymbol{b}_m) \tag{24}$$

where $\boldsymbol{b}_m$ is found by solving the gradient of a truncated series expansion of a geomagnetic potential function:

$$V = a \sum_{n=1}^{N} \sum_{m=0}^{n} \left(\frac{a}{r_m}\right)^{n+1} \left[g_n^m \cos(m\phi) + h_n^m \sin(m\phi)\right] P_n^m(\cos\theta) \tag{25}$$

The Gauss coefficients are determined through measurements and are updated every five years by the International Association of Geomagnetism and Aeronomy (IAGA). The series is available to degree and order 10 (120 coefficients) (data available online at http://www.ngdc.noaa.gov/IAGA/wg8/igrf2000.html [cited 30 June 2003]). Solutions to the gradient of this expansion are available in C, FORTRAN, and MATLAB® from the National Space Science Data Center (data available online at http://nssdcftp.gsfc.nasa.gov/models/geomagnetic/igrf/ [cited 30 June 2003]).

To avoid computing matrix inverses, each individual component of the measured field vector can be processed by itself. Essentially, each reported component of the measured magnetic field vector is treated as an individual sensor and processed accordingly. This not only allows for the attitude to be solved without computing a matrix inverse, but also allows for attitude solutions even if some components of the magnetometer measurement are not available. Therefore, h is the component of $\boldsymbol{b}_m^{\text{rot}}$ that corresponds to the measurement component currently being evaluated. There are now three derivations of $\boldsymbol{H}$ to relate it to the three different vector components:

$$\boldsymbol{H}_x^T = 2\begin{bmatrix} 2x_1b_1 - x_3b_3 + x_4b_2 \\ 2x_2b_1 + x_3b_2 + x_4b_3 \\ x_2b_2 - x_1b_3 \\ x_2b_3 + x_1b_2 \\ 0 \\ 0 \\ 0 \end{bmatrix}$$

$$\boldsymbol{H}_y^T = 2\begin{bmatrix} 2x_1b_2 - x_4b_1 + x_2b_3 \\ x_3b_1 + x_1b_3 \\ 2x_3b_2 + x_2b_1 + x_4b_3 \\ x_3b_3 - x_1b_1 \\ 0 \\ 0 \\ 0 \end{bmatrix}$$

$$\boldsymbol{H}_z^T = 2\begin{bmatrix} 2x_1b_3 - x_2b_2 + x_3b_1 \\ x_4b_1 - x_1b_2 \\ x_4b_2 + x_1b_1 \\ 2x_4b_3 + x_2b_1 + x_3b_2 \\ 0 \\ 0 \\ 0 \end{bmatrix} \tag{26}$$

The subscripts refer to the components of the vectors involved and $\boldsymbol{H}_x$, $\boldsymbol{H}_y$, and $\boldsymbol{H}_z$ correspond to the x, y, and z components of the magnetic field vector.

Simulation

To simulate the magnetometer measurements, the International Geomagnetic Reference Field (IGRF) model was used. Magnetometer measurements are considered to be very accurate (usually within 0.3 mG). The model of the Earth's magnetic field, however, is not as accurate. The errors are nonlinear and orbit dependent.[18] In an attempt to model this type of behavior, the "true" magnetic field was modelled using a 10th-order IGRF model with coefficients from the year 2000. The measurements were created by using a sixth-order IGRF model with coefficients from 1995 and adding a zero mean white-noise Gaussian process with a standard deviation of 0.3 mG. It was assumed that all biases had been correctly calibrated out of the system. This type of simulation was previously utilized by Crassidis and Lightsey[19] and is typically used to simulate magnetometer sensor errors.

Results

With the magnetometer measurements related to the state vector, it is possible to combine them with the SNR and carrier-phase measurements. Two separate circumstances were evaluated. In one, it was assumed that only one antenna boresight vector was available to combine with the magnetometer data. This situation would arise if only one GPS antenna were utilized, or if the antennas of an array were aligned. The second circumstance combined magnetometer data with the SNR and carrier-phase measurements from a canted array.

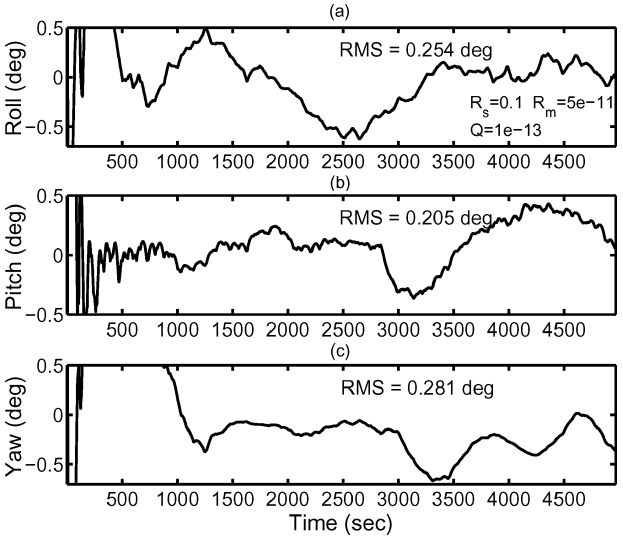

Fig. 14 Combined SNR and magnetometer attitude error: a) roll, b) pitch, and c) yaw.

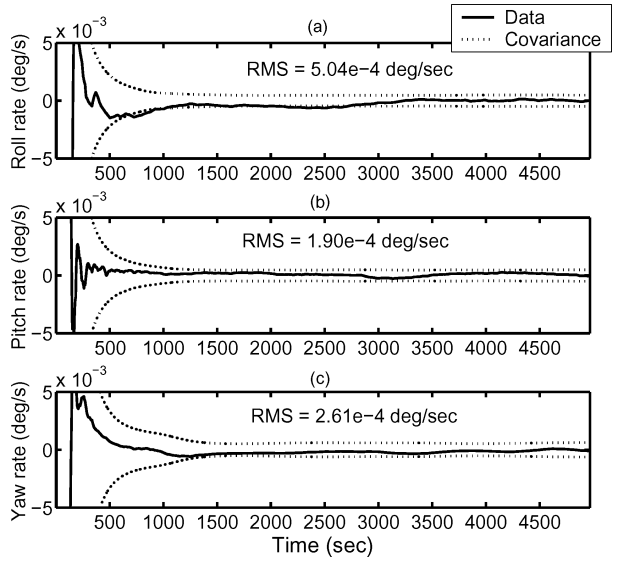

Fig. 15 Combined SNR and magnetometer body rate error with covariance: a) roll rate, b) pitch rate, and c) yaw rate.

Table 5 Integer resolution comparison: SIGI receiver with and without magnetometer measurements (orbit simulation)

Configuration	Calibration	Correct integer estimation, %	Initial correct estimate, s
Without magnetometer	No	51.0	40
Without magnetometer	Yes	53.2	4
With magnetometer	No	84.3	11
With magnetometer	Yes	88.4	9

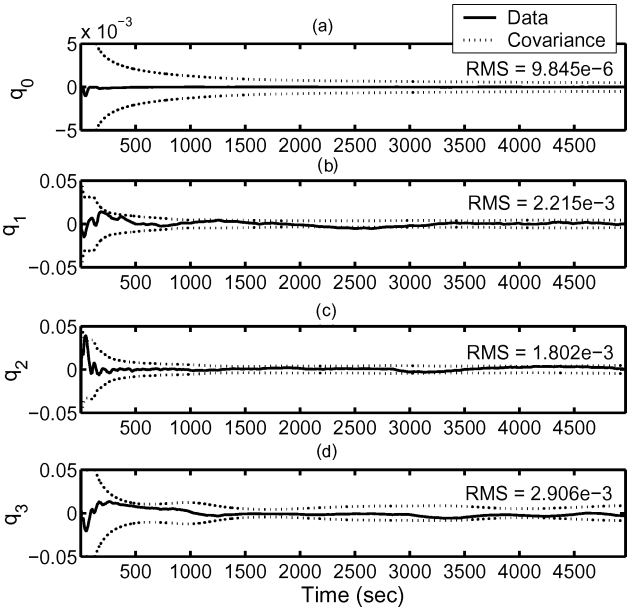

Fig. 16 Combined SNR and magnetometer quaternion error with covariance: a) q_0, b) q_1, c) q_2, and d) q_3.

For the single-antenna case only SNR measurements were processed from a Mitel Architect receiver in an orbit simulation. Similar to the pivot, this single-antenna receiver performs a more precise measurement of SNR than the SIGI. After iteration, values for the sensor noise r of the SNR measurements and the magnetometer measurements r_{mag}, along with a process noise covariance value $\boldsymbol{Q}$, were found, which gave good results. The filter provided rms attitude error values of 0.254, 0.205, and 0.281 deg in roll, pitch, and yaw and converged to correct values of the body rates. The results are shown in Figs. 14–16. Integers could easily be resolved at this level of accuracy for an aligned antenna array.

For the case of multiple canted antennas, the SIGI receiver was used in an orbit simulation. The addition of the magnetometer measurements improves the integer resolution accuracy. The correct integer estimation test was performed again. A comparison of the integer estimation accuracy with and without magnetometer measurements appears in Table 5 and demonstrates a significant improvement in integer resolution when the magnetometer was added to the system.

Conclusions

This research has demonstrated how utilizing SNR measurements from canted antennas can accurately and rapidly resolve the integer ambiguities for double-difference carrier-phase measurements. In all of the tests that were performed, the integers were correctly assigned in less than 1 min. In several circumstances the integers were resolved in less than 30 s. This work has further shown that using canted antennas does not appear to have a significant effect

on the double-difference carrier-phase measurements. The experiments conducted on the roof indicate that this algorithm can provide attitude estimates that are generally less than 0.5 deg in error in a noisy environment with antenna baselines of 1 m.

As expressed in the text, the SIGI receiver utilized for the validation of this algorithm is not the most effective receiver for this type of algorithm. The SIGI SNR measurements are not very precise. Future work could validate the performance of the algorithm using a receiver that made a more precise SNR measurement and had more channels available to track GPS satellites. Based on the work done with the PiVoT receiver, it is anticipated that a different receiver could produce results superior to those presented here. It might also be possible to improve the results through additional filtering techniques. Line bias estimation, multipath modelling, and exponentially correlated random variables might all improve the solution accuracy. Because the accuracy required to correctly resolve the integers is a function of line-of-sight geometry, it might be possible to further improve the integer resolution procedure by a judicious choice of the order in which carrier-phase measurements are processed.

The addition of the magnetometer demonstrated how integer resolution can be performed with a more traditional aligned array if an additional sensor is used. The tests also demonstrated how additional sensor data can improve the integer resolution for the canted antenna case. The tests with the Mitel Architect receiver lead to the conclusion that an accurate measure of SNR could generate nearly 100% correct integer estimation in some cases.

Acknowledgment

The authors acknowledge the support of NASA's Goddard Space Flight Center. Their financial support made this research possible, and the multiple-antenna simulations were carried out in their GPS laboratory.

References

[1]Lightsey, E. G., "Development and Flight Demonstration of a GPS Receiver for Space," Ph.D. Dissertation, Dept. of Aeronautics and Astronautics, Stanford Univ., Stanford, CA, Feb. 1997.

[2]Axelrad, P., and Ward, L. M., "Spacecraft Attitude Estimation Using the Global Positioning System: Methodology and Results for RADCAL," *Journal of Guidance, Control, and Dynamics*, Vol. 19, No. 6, 1996, pp. 1201–1209.

[3]Carpenter, J. R., and Hane, R. M., "Precise Evaluation of Orbital GPS Attitude Determination on the STS-77 GPS Attitude and Navigation Experiment (GANE)," *Proceedings of the ION National Technical Meeting*, Inst. of Navigation, Fairfax, VA, 1997, pp. 387–398.

[4]Brock, J. K., Fuller, R., Kemper, B., Miezcko, D., Rodden, J., and Tadros, A., "GPS Attitude Determination and Navigation Flight Experiment," *Proceedings of the ION GPS*, Inst. of Navigation, Fairfax, VA, 1995, pp. 545–554.

[5]Ward, L. M., "Spacecraft Attitude Estimation Using GPS: Methodology and Results," Ph.D Dissertation, Dept. of Aerospace Engineering Science, Univ. of Colorado, Boulder, CO, Aug. 1996.

[6]Melvin, P. J., Ward, L. M., and Axelrad, P., "The Analysis of GPS Attitude Data from a Slowly Rotating, Symmetrical Gravity Gradient Satellite," *Journal of Astronautical Sciences*, Vol. 44, No. 4, 1996, pp. 515–539.

[7]Ward, L. M., and Axelrad, P., "A Combined Filter for GPS-Based Attitude and Baseline Estimation," *Navigation: Journal ION*, Vol. 44, No. 2, 1997, pp. 195–213.

[8]Axelrad, P., and Behre, C. P., "Satellite Attitude Determination Based on GPS Signal-to-Noise Ratio," *Proceedings of the IEEE*, Vol. 77, No. 1, 1999, pp. 122–144.

[9]Dunn, C., and Duncan, C., "Estimating Attitude From GPS Measurements on One Antenna," NASA Technical NPO 20323 Briefs, June 1998.

[10]Buist, P. J., Hashida, Y., Unwin, M., and Schroeder, M., "Spacecraft Full Attitude Determination from a Single Antenna: Experimentation with the PoSAT-1 GPS Receiver," *Proceedings of the ION Technical Meeting*, Inst. of Navigation, Fairfax, VA, 1998, pp. 1811–1817.

[11]Lightsey, E. G., and Madsen, J. D., "3-Axis Attitude Determination Using Global Positioning System Signal Strength Measurements," *Journal of Guidance, Control, and Dynamics*, Vol. 26, No. 2, 2003, pp. 304–310.

[12]Madsen, J. D., "Obtaining 3-Axis Attitude Solution from GPS Signal to Noise Ratio Measurements," *Proceedings of the ION GPS*, Inst. of Navigation, Fairfax, VA, 2001, pp. 2927–2936.

[13]Gelb, A., *Applied Optimal Estimation*, MIT Press, Cambridge, MA, 1994, p. 188.

[14]Kuipers, J. B., *Quaternions and Rotation Sequences—A Primer with Applications to Orbits, Aerospace and Virtual Reality*, Princeton Univ. Press, Princeton, NJ, 2002, p. 127.

[15]Madsen, J. D., "Use of Kalman Filtering Techniques on a Signal to Noise Ratio Attitude Estimation Algorithm for the International Space Station," M.S. Thesis, Dept. of Aerospace Engineering and Engineering Mechanics, Univ. of Texas, Austin, TX, Aug. 2000.

[16]Wennersten, M. D., Banes, A. V., Boegner, G. J., Dougherty, L., Edwards, B. L., and Roman, J., "PiVoT GPS Receiver," *Proceedings of the ION GPS*, Inst. of Navigation, Fairfax, VA, 2001, pp. 855–861.

[17]Butsch, F., "A Growing Concern Radiofrequency Interference and GPS," *GPS World*, Vol. 13, No. 10, 2002, pp. 40–49.

[18]Crassidis, J. L., Andrews, S. F., Markley, F. L., and Ha, K., "Contingency Designs for Attitude Determination of TRMM," *Proceedings of the Flight Mechanics Estimation Theory Symposium*, NASA Goddard Space Flight Center, Greenbelt, MD, 1995, pp. 419–433.

[19]Crassidis, J. L., and Lightsey, E. G., "Attitude Determination Using Combined GPS and Three-Axis Magnetometer Data," *Space Technology: Journal of the International Forum on Automatic Control*, Vol. 20, No. 4, 2001, pp. 147–156.

D. Spencer
Associate Editor